Unsteady granular flows in a rotating tumbler

Nicholas A. Pohlman[*]

Department of Mechanical Engineering, Northern Illinois University, DeKalb, Illinois 60015, USA

Julio M. Ottino

Department of Chemical and Biological Engineering, Department of Mechanical Engineering,
The Northwestern Institute on Complex Systems (NICO), Northwestern University, Evanston, Illinois 60208, USA

Richard M. Lueptow

Department of Mechanical Engineering, Northwestern University, Evanston, Illinois 60208, USA

The characteristics of steady granular flow in quasi-two-dimensional rotating tumblers have been thoroughly investigated and are fairly well understood. However, unsteady time-varying flow has not been studied in detail. The linear response of granular flow in quasi-two-dimensional rotating tumblers is presented for periodic forcing protocols via sinusoidal variation in the rotational speed of the tumbler and for step changes in rotational speed. Variations in the tumbler radius, particle size, and forcing frequency are explored. Similarities to steady flow include the fastest flow occurring at the free surface of the flowing layer and an instantaneous approximately linear velocity profile through the depth. The flowing layer depth varies by 2–5 particle diameters between minimum and maximum rotation rates. However, unsteady forcing also causes the flow to exhibit dynamic properties. For periodic rotational speeds, the phase lag of the flowing layer depth increases linearly with increasing input forcing frequency up to nearly 2.0 rad over 0–20 cycles per tumbler revolution. The amplitude responses of the velocity and shear rate show a resonance behavior unique to the system level parameters. The phase lag of all flow properties appears to be related to the number of particle contacts from the edge of the rotating tumbler. Characterization via step changes in rotational speed shows dynamic properties of overshoot (up to 35%) and rise times on the order of 0.2–0.7 s. The results suggest that the unsteady granular flow analysis may be beneficial for characterizing the "flowability" and "rheology" of granular materials based on particle size, moisture content, or other properties.

PACS number(s): 45.70.Mg, 47.57.Gc, 83.80.Fg

I. INTRODUCTION

The development of new experimental, theoretical, and computational approaches has, over the last two decades, provided an understanding of several fundamental aspects of the physics of granular flow. Experimental techniques based on particle image velocimetry, particle tracking, and magnetic-resonance imaging have provided information about the velocity and number density profiles over a wide range of conditions [1,2]; continuum and rheological theories have provided the basis for models of granular flows [3,4], and particle dynamics simulations and increased computational speeds have permitted the direct simulation of granular flows [5,6]. However, with the exception of intermittent avalanche flows, most work has focused on steady or quasi-steady granular flow. In this paper, we consider unsteady granular flow in a continuously flowing layer.

Steady flow in a flowing layer is reasonably well understood. For instance, the shear rate is approximately constant and the fastest velocities occur at the free surface [2,7–9]. Some work has explored the transition from static conditions to fully developed flow using dynamic properties of granular materials and the knowledge of interparticle static friction to relate these two states [10]. Others have considered the de-

velopment of the velocity profile within an avalanche as well as the time to reach to static equilibrium after the avalanche stops [11,12]. While avalanches represent intermittent flow of particles, here we consider the response of granular materials as they experience transient forcing conditions yet maintain continuous flow.

Prior experiments measuring granular velocity in transient forcing conditions have been conducted in annular and Couette-type shear cell devices [13–16]. The primary emphasis was exploring how the bulk material approaches steady-state conditions relative to the starting static equilibrium. In a Couette shear cell, the previous direction of flow strongly influences the time to recover force networks and flow conditions of steady state when the system is restarted. When the applied force is in the same direction as the previous flow, the shear stress and column height immediately reach steady-state conditions, whereas when the applied force is in the opposite direction, the granular material needs 5–10 revolutions of the inner cylinder to reacquire steady-state conditions [15]. Additionally, when the inner cylinder is oscillated, the continuous reorganization within the bulk of the granular material increases the packing density over time. This effect is much like what occurs in tapping experiments of granular materials, where the forcing is a periodic impact to a container, typically via a hammer or mallet [17–19].

Prior research on transient flow in rotating tumblers has been limited to axial flow conditions (transverse the primary flow direction) during the startup of rotary kilns [20–23].

*npohlman@niu.edu

Some research has been done to characterize the thickness of the flowing layer as a function of the changing orientation for unique cross-sectional shapes [24]. Other dynamic conditions studied in rotating tumblers are the appearance and evolution of segregation bands (both radially [25–27] and axially [28–31]) for bidisperse mixtures of particles. For experiments using constant rotation rates, the transient effects are related to the coarsening of the segregated regions of the tumbler over time scales on the order of hundreds of tumbler rotations. Some experiments, however, explicitly use transient flow conditions, either a periodically varying rotation rate or a polygonal container rotating at a constant angular velocity, to generate unique lobed segregation patterns for bidisperse mixtures in a quasi-two-dimensional (quasi-2D) tumbler [25,32]. A simple model effectively predicts the number of segregation lobes based on the frequency of a periodic forcing protocol [25,33]. This model explicitly assumes instantaneous responses in flow velocity and flowing layer depth with the time-varying rotation rate. However, there is no experimental justification for this assumption.

This provides the motivation for this investigation of granular flow in quasi-two-dimensional rotating tumblers with transient forcing. The circular tumbler geometry is used because the flow characteristics in quasi-two-dimensional rotating tumblers have been well documented for steady flow conditions, though details of quasi-2D flows deviate slightly from fully three-dimensional flow at the center of an infinitely long tumbler due to sidewall interactions [2,7,8,34]. The focus of this paper is to investigate the linear response of the velocity and shear rate in the flowing layer and the thickness of the flowing layer as the speed of the tumbler changes within the continuous flow regime. Parameters that are varied include the radius of the tumbler, the size of the particles, and, most importantly, the frequency of the forcing.

II. EXPERIMENTAL SETUP

The transient velocity response to changes in the forcing parameters was experimentally measured via particle tracking velocimetry (PTV) [2,35] in quasi-2D rotating tumblers of various diameters. In a quasi-2D system where the tumbler thickness L is only a few particle diameters, the free-surface flow can be viewed from the end wall of the container, as shown in Fig. 1.

The particle positions were made visible through a flash from a 25 mJ Nd:YAG laser beam (New Wave Research) impinging on a diffuser plate. Images were recorded with a 1 megapixel charged coupled device (CCD) camera (TSI, Inc.) that was synchronized with the laser flashes. Recording images through the clear end wall of the tumbler allowed measurement of the flow velocities through the depth of the flowing layer, similar to previous experiments [2,8,36]. The measurements were obtained only for those particles adjacent to the end wall, but the short axial thickness limited the potential for the three dimensionality of the flow [34].

The tumblers were constructed from a sandwich of several acrylic sheets of varying thickness with a circular portion of either radius $R=8.6$ or radius $R=13.9$ cm removed from the center of the sheets. Images were recorded at the
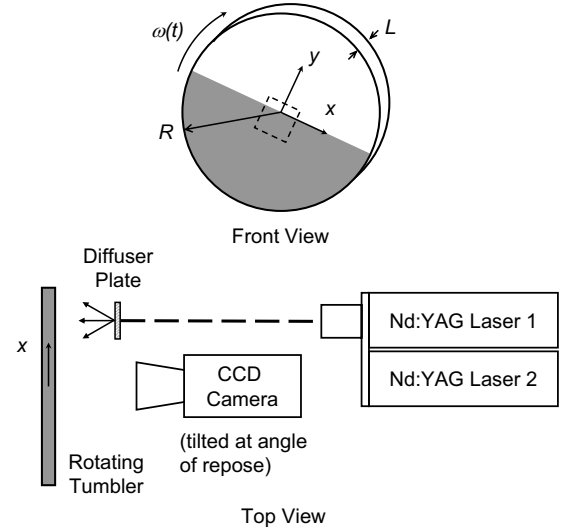

FIG. 1. Schematic of a half-filled quasi-2D tumbler parameters (front view) with radius R, axial thickness L, rotation rate $\omega(t)$, and the coordinate system at the midlength of the flowing layer. The dashed box represents the area of the flowing layer that was investigated at $x=0$. The top view shows the rotating tumbler position relative to the CCD camera, the diffuser plate, and the dual-head laser light source (not to scale).

midlength of the flowing layer. The front and back walls of the tumbler were made of 6.4-mm-thick, clear, and static-dissipative acrylic in order to view the particles within the tumbler. Multiple sheets with the circular cut outs were combined between the end plates to create axial thickness $L\approx9d$ (where d is the particle diameter). The tumbler was filled to a 50% volume fraction with monodisperse black basalt glass particles of either $d=1.07\pm0.04$ mm or 2.03 ± 0.03 mm. The black particles produced a strong single reflection point of the laser light with very little background reflection. Black cloth was placed between the back end wall and the mounting hardware in order to minimize background optical noise in the image. The interior portion of the tumbler was cleaned with an antistatic wipe prior to filling the tumbler.

The acrylic sheets were fixed to an aluminum back plate attached to a brushless dc stepper motor. The velocity of the motor was controlled so that the tumbler speed could be varied following a trigger from the image acquisition system. Two forms of forcing were implemented: a single frequency sinusoidal protocol and an abrupt step change in rotational speed. The sinusoidal time-dependent rotational speed was

$$\omega(t) = \begin{cases} \omega_{\mathrm{o}} - \omega_A & (t<0) \\ \omega_{\mathrm{o}} - \omega_A \cos(2\pi n\omega_{\mathrm{o}}t) & (t\geq0), \end{cases} \quad (1)$$

where ω_{o} is the average rotational speed in revolutions per second, ω_A is the amplitude of the periodic oscillation [$\omega_A < \omega_o$ causing $\omega(t)>0$ at all time steps producing continuous tumbler rotation in the same direction], and n is an integer number of periodic oscillations during each revolution of the tumbler, with $n=\{3,6,10,13,16,20\}$ such that the tumbler rotation rate is the same at the beginning and end of one full

tumbler revolution. The values of ω_o, ω_A, and size of the step increase are based on a minimum speed of Fr=10^{-4} and a maximum speed of Fr=10^{-3}, where Fr=$R(2\pi\omega)^2/g$ is the Froude number. This corresponds to ω_o=0.035 4 rev/s and ω_A=± 0.018 4 rev/s for R=8.6 cm and ω_o =0.027 8 rev/s and ω_A=± 0.014 4 rev/s for R=13.9 cm. For the range of Froude numbers used in these experiments, the flowing layer was in the continuous flow regime with a flat free surface [37,38].

To allow ensemble averaging, 20 separate experimental runs for each combination of tumbler diameter, particle size, and forcing oscillation frequency were recorded and analyzed using PTV. Each image pair and PTV result were individually verified for accuracy to avoid any false PTV calculations. Accuracy of the PTV measurements based on particle location to less than 10% subpixel resolution, the pixel to length conversion, and the laser flash/camera timing uncertainty of 200 ns yields a typical overall uncertainty of ± 1.6 mm/s for 1 mm particles and ± 2.5 mm/s for 2 mm particles for the worst case for extremely slow moving particles. The time separation of the PTV dual-head laser flash ranged from 0.9 to 3.4 ms, while the frequency of image pair acquisition was between 3 and 15 Hz, depending on experimental conditions. The frequency of image pair acquisition was adjusted such that two to five periods of the forcing protocol were recorded during an individual run. The velocity vectors at each of the time steps for 20 runs were then sorted into one-particle diameter wide bins in the y direction and extending the streamwise length of the image (about $10d$). The coordinate system was always oriented along the instantaneous flat free surface of the flowing layer. The streamwise and transverse velocities in each bin were averaged for each time step to provide the time-varying velocity through the depth of the flowing layer. Velocities more than five standard deviations away from the local mean were recursively removed from the data sets to eliminate any erroneous PTV calculations. This resulted in the removal of less than 0.5% of the approximately 7×10^6 total available vectors.

III. RESULTS

A. Velocity and depth of flowing layer

The streamwise velocity through the flowing layer $u(y)$ responds to the rotational speed of the tumbler in a manner that mimics the forcing protocol, as shown in Fig. 2. The figure shows the forcing [in terms of $\omega(t)$ and Fr] in the upper graph and a typical streamwise velocity response throughout the flowing layer in the lower graph. Similar velocity responses are observed for all particle sizes, tumbler diameters, and forcing frequencies. The topmost layer of particles exhibits the fastest streamwise flow velocity at all time steps with decreasing velocity through the depth of the flowing layer. The streamwise velocity follows the sinusoidal forcing at all depths in the flowing layer. The transverse velocity in the flowing layer is negligible, consistent with prior results for steady flow in quasi-2D tumblers [2,8].

The instantaneous velocity profiles through the flowing layer $u(y/d)$ are shown in Fig. 3. The left graph shows the
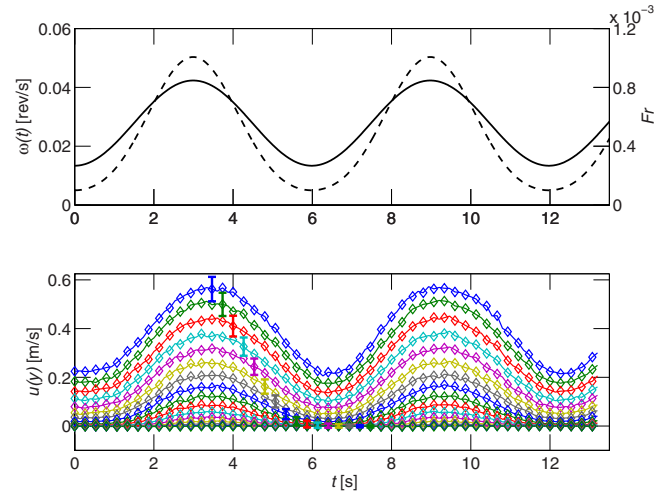

FIG. 2. (Color online) Periodic forcing protocol (top) in terms of rotational speed ω (solid curve; left axis) and Fr (dashed curve; right axis) for tumbler frequency n=6. The streamwise velocity response u (bottom) in the R=13.9 cm, L=0.9 cm tumbler with 1 mm particles. Each curve on the velocity plot is for an individual one-particle-diameter-thick layer in the flow with the upper most curve indicating the streamwise velocity at the free surface. The lower curves indicate the velocity response at increasing depths through the flowing layer. Markers are only shown for half of the time steps for clarity, and standard deviations of the ensemble averaging for each layer are shown starting at t=3.5 s.

streamwise velocity profile from $6.3 \leq t \leq 8.9$ s, in which the speed of the flowing layer is increasing; the right graph shows the flowing layer profile for decreasing velocity from $8.9 \leq t \leq 12.3$ s. The closely spaced velocity profiles represent the extrema of velocities in the flowing layer, while those profiles with large separation occur during maximum acceleration and deceleration in the flowing layer. The velocity profiles for accelerating and decelerating flows are nearly
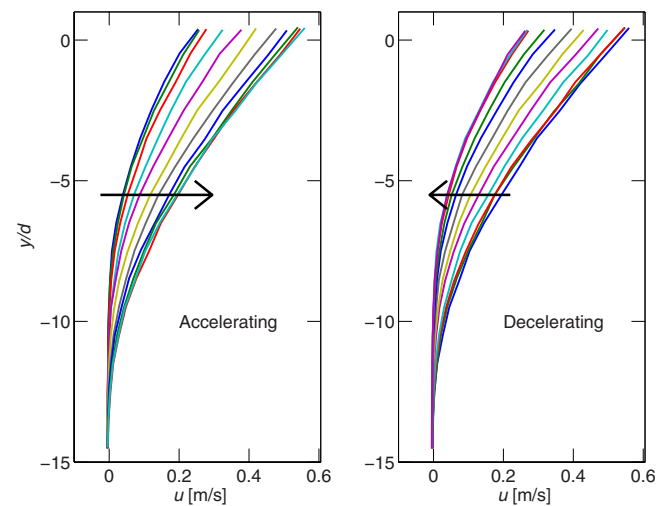

FIG. 3. (Color online) Streamwise velocity profile $u(y/d)$ through the flowing layer for accelerating flow (left) and decelerating flow (right). Conditions are the same as Fig. 2 with R=13.9 cm, L=0.9 cm, and 1 mm particles. The arrows indicate increasing time.
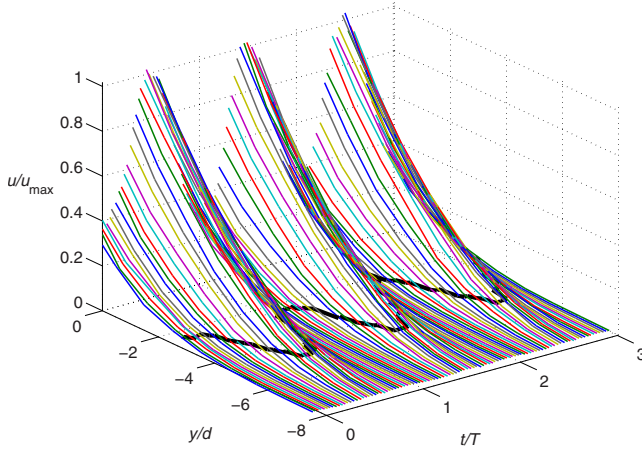
FIG. 4. (Color online) Streamwise velocity profile at each time step (relative to period of oscillation $T=\frac{1}{n\omega_o}$) as a function of the flowing layer depth (in terms of number of particle diameters) in the $R=8.6$ cm, $L=1.8$ cm tumbler with 2 mm particles and $n=13$. The maximum streamwise velocity is $u_{\max}=0.25$ m/s. The black curve at the zero velocity plane is the calculated flowing layer depth δ.

identical with residual differences yielding $R^2>0.985$ when considering the closest match to the maximum streamwise velocity. At all times, the streamwise velocity profile is approximately linear from the free surface through the upper half of the depth of the flowing layer, which is consistent with previous results for steady flows [2,8], giving way to a nonlinear decay deeper in the flowing layer until the velocity is negligible. The depth where this decay occurs fluctuates with time, corresponding to the growing and shrinking thickness of the flowing layer.

From Figs. 2 and 3, it is evident that the flowing layer depth increases to about $12d-13d$ at the high rotational speed and decreases to $8d-9d$ at the low rotational speed. Similar results occur for all tumbler radii, particle sizes, and forcing frequencies. The effect is shown more clearly in Fig. 4, in which the flowing layer streamwise velocity profile $u(y)$ is shown at each time step for the $R=8.6$ cm, $L=1.8$ cm tumbler with 2 mm particles, and a forcing frequency of $n=13$. Assuming a linear velocity profile in the upper portion of the flowing layer at any time step, the shear rate $\dot{\gamma}$ and a measure of the flowing layer depth δ can be calculated from a fit of the data to a velocity profile of the form,

$$u(y) = \dot{\gamma}(y - \delta), \tag{2}$$

where δ is simply the depth at which a linear velocity profile fit has a value of zero. This definition of δ is more robust than measuring the point of zero velocity because of the difficulty in accurately measuring velocities in the extremely slow flow in the lower portion of the flowing layer. Only those bins with particles flowing at a velocity greater than the minimum PTV resolution (approximately 5 particle diameters per second) were used in the fit to the linear velocity profile. The coefficient of determination of the linear regression fit for the different combinations of particle size,
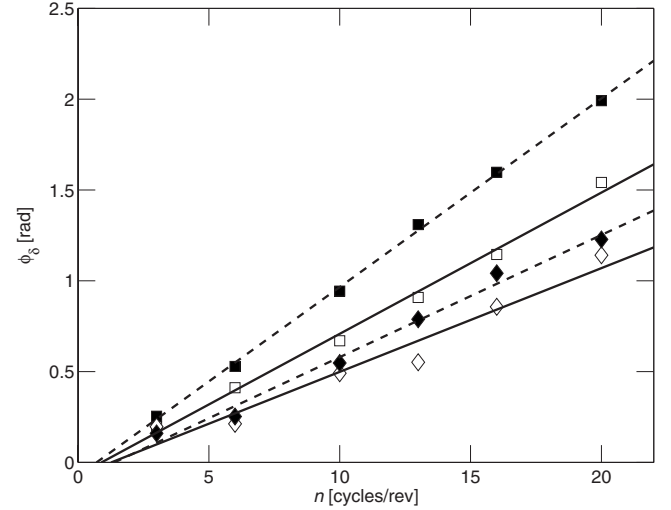

FIG. 5. Phase lag of the sinusoidal response of the flowing layer depth ϕ_δ increases linearly as a function of the forcing frequency. ($\square$) $d=1$ mm particles and ($\diamond$) $d=2$ mm particles; open markers represent tumbler radius $R=8.6$ cm and filled markers represent $R=13.9$ cm.

tumbler dimension, and forcing frequency was $0.95\le R^2 \le 0.97$, confirming the linear form of Eq. (2).

Using Eq. (2), the flowing layer depth δ at each time step is shown as the black curve at the base of the velocity profiles in Fig. 4. In this example, the larger particles and smaller tumbler radius cause the flowing layer depth to oscillate between $2.5d$ and $5.5d$ compared to $8.5d$ to $12.5d$ for $R=13.9$ cm, $d=1$ mm shown in Fig. 2. The variation in the flowing layer depth with tumbler speed confirms that validity of this assumption, which has been used in a model to predict lobed segregation structures from periodic forcing in circular tumblers [25].

B. Linear response of a granular flow

The changes in the dynamic response of the granular flow to the sinusoidal forcing protocol, particularly the amplitude and phase, are of key interest. Here we consider the response of the granular flow in terms of flowing layer depth δ, shear rate $\dot{\gamma}$, and streamwise velocity u. Given the sinusoidal form for the forcing, a linear response would be of the form

$$\psi(t) - \psi_o = \Lambda_\psi \cos(\varpi_\psi t - \phi_\psi), \tag{3}$$

where the Λ is amplitude, ϖ is the frequency, ϕ is the phase lag (with respect to the forcing), and $\psi(t)$ can be the shear rate $\dot{\gamma}$, the flowing layer depth δ, or the streamwise velocity u (with ψ_o as the corresponding mean value). The variables of Eq. (3) are determined from a nonlinear least-squares fit to the data.

In all cases, the response frequency $\varpi_{\dot{\gamma},\delta,u}$ matches the input frequency determined from the number of cycles per revolution of the tumbler within 2.5% or less. The amplitude of the flowing layer depth Λ_δ ranges from 0.60 to 1.55 particle diameters, but no clear relation to the forcing frequency was evident. The phase lag ϕ_δ, however, increases nearly linearly as the forcing frequency increases shown in Fig. 5,
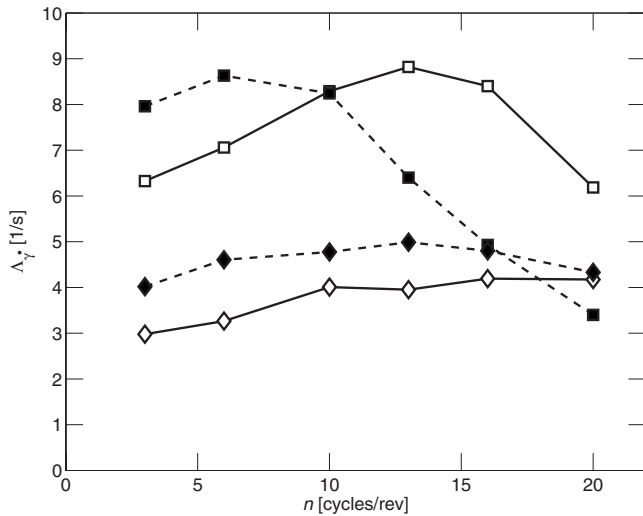
FIG. 6. Amplitude of sinusoidal response of the shear rate $\Lambda_{\dot{\gamma}}$ as a function of the forcing frequency. ($\square$) $d=1$ mm particles and ($\lozenge$) $d=2$ mm particles; open markers represent tumbler radius $R=8.6$ cm and filled markers represent $R=13.9$ cm; the curves for each radius-particle size combination are guides for the eyes.

indicating the delay in the response of the granular flow to the forcing. The magnitude of phase lag depends on the tumbler diameter and particle size. For a constant particle size, the phase lag increases with increasing tumbler radius, as would be expected given the greater radial distance from the center of the tumbler to the tumbler wall and the corresponding number of particle contacts required to transmit operating conditions (i.e., changes in rotation rate) to the flow in the center of the tumbler. Likewise, for constant radius, the phase lag decreases with increasing particle size. Larger particles require fewer contacts to transmit changes in the tumbler speed to the flow and therefore respond with less phase lag than small particles for which more interparticle contacts must occur. Lastly, the intercept with zero phase lag for the fitted lines occurs at a positive nonzero forcing frequency of approximately $n \approx 1$. This indicates that a threshold exists below which the flow response is fast enough that the forcing is felt nearly instantaneously throughout the flowing layer.

The phase lag for the response of the shear rate $\phi_{\dot{\gamma}}$ to sinusoidal forcing frequency is similar to that for the flowing layer depth shown in Fig. 5. However, the amplitude of the shear rate response $\Lambda_{\dot{\gamma}}$ suggests a resonancelike behavior, as shown in Fig. 6. For example, the maximum shear rate amplitude for the $R=13.9$ cm, $d=1$ mm condition is at $n=6$ cycles per tumbler revolution and then decreases by more than half as the forcing frequency increases to $n=20$. The "resonance" shifts to a higher frequency $n=13$, for the smaller radius tumbler, and then follows the same pattern of decreasing amplitude with increasing forcing frequency. A resonance peak is not clearly evident for the tumblers with larger $d=2$ mm particles, though there appears to be a broad maximum in the response. Additionally, the maximum resonance amplitudes of $d=2$ mm particles are approximately half of those observed for $d=1$ mm particles. This difference in magnitude of the shear rate amplitude may result from the greater "fluidity" of smaller particles relative to larger par-

ticles [2]. The small particles may be more susceptible to acceleration and deceleration as a consequence of their smaller inertia. With the lower overall shear rate amplitude for the $d=2$ mm particles, the magnitude of the attenuation at higher forcing frequencies is not as dramatic as for smaller particles.

To get a better sense of the relative influence of the dynamic parameters of amplitude response and phase lag, the streamwise velocity scaled by the maximum velocity for each tumbler radius and particle size combination is plotted for a single oscillation of the rotational speed of the tumbler shown in Fig. 7, where $T=\frac{1}{n\omega_o}$ is the period of oscillation.

The changes in amplitude response with respect to the forcing frequency are relatively subtle with the most clear resonance shown for the $R=8.6$ cm, $d=1$ mm case [Fig. 7(a)]. Similar to the amplitude of the shear rate, the maximum amplitude of the velocity response occurs at forcing frequency $n=13$, as indicated by the velocity of the top layer reaching the horizontal dashed line representing unit dimensionless velocity. The velocity response is slightly attenuated for $n < 13$ and $n > 13$, as the oscillations do not quite reach the unit dimensionless velocity dashed lines. Deeper in the flowing layer, differences in the velocity response to the forcing frequency are less obvious. This is reasonable given the slower velocity closer to the interface of the flowing layer and fixed bed, where the highly energetic dynamically responsive free-surface flow is constrained by the quasistatic nature of the fixed bed.

More evident in Fig. 7 is the increasing phase lag of the velocity response with increasing forcing frequency. This is most clearly observed when comparing the forcing sinusoid at the top of each graph to the sinusoidal wave forms of velocity for various values of the forcing frequency. The circles on the red curve connect the wave form peaks for the sinusoidal fit to the velocity response at the free surface for all forcing frequencies n. Consistent with the flowing layer depth data in Fig. 5, the greatest phase lag for the velocity occurs for the $R=13.9$ cm, $d=1$ mm case, and all cases show a nearly linear increase in phase lag as a function of the forcing frequency.

Another trend evident in Fig. 7 is the decreasing phase lag as a function of increasing depth through the flowing layer, as indicated by the black vertical curve for each forcing frequency condition. The general decrease in the phase lag through the depth, particularly for high forcing frequencies, suggests that particles deeper in the flowing layer respond more quickly than those at the free surface due to their close proximity to the fixed bed.

C. Linear response of flow to a step input

The previous sections reported results for sinusoidal forcing at a single frequency. To characterize many frequencies simultaneously, experiments were conducted for the transient response to step changes in the rotational speed of the tumbler. The same dimensionless slow (Fr$=10^{-4}$) and fast (Fr$=10^{-3}$) rotational speeds of the tumbler were used in order to maintain a continuous flat flowing layer. After the
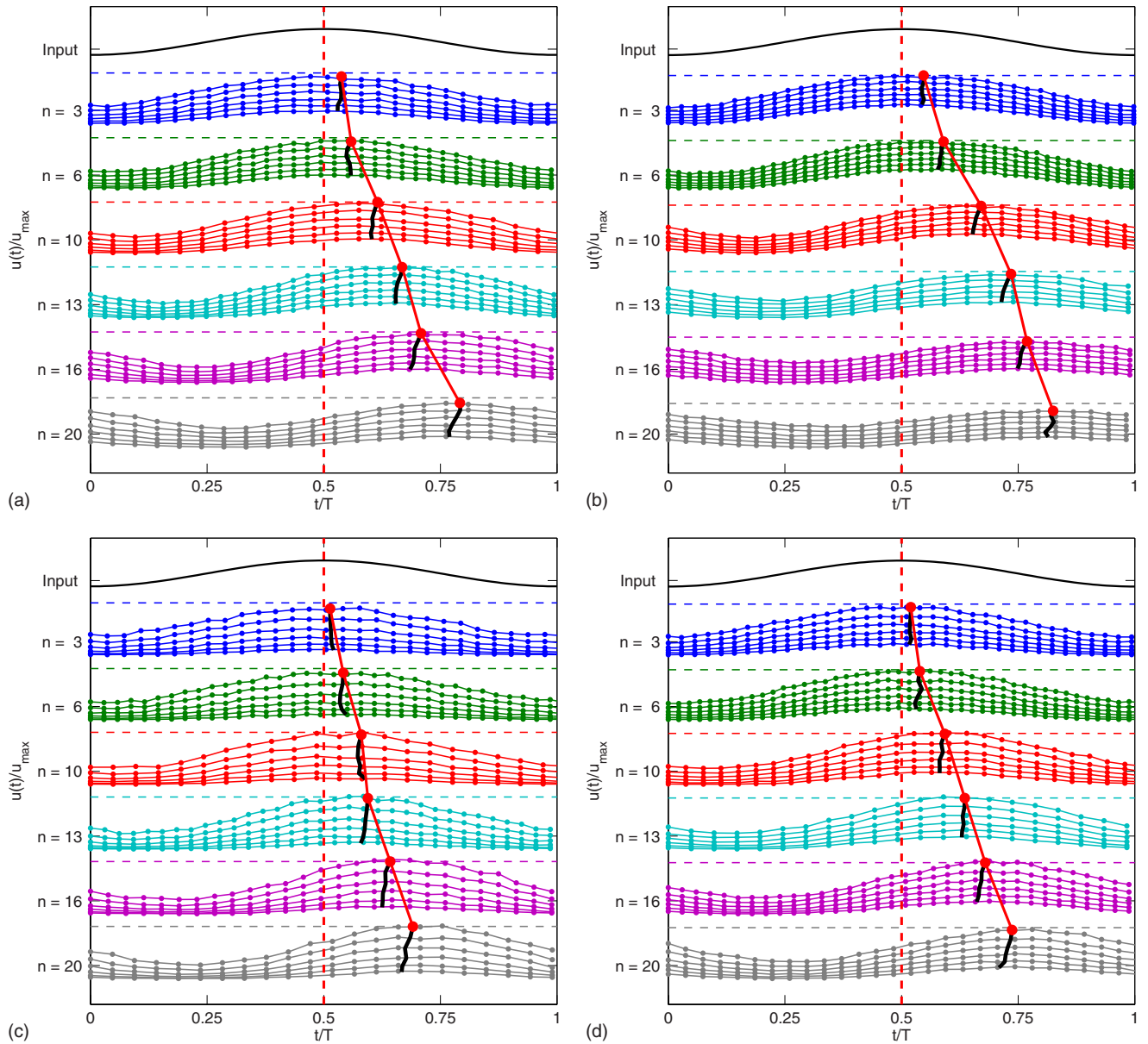
FIG. 7. (Color online) Response of the streamwise velocity scaled by the maximum velocity for the top six single-particle-diameter-thick layers (timing resolution does not provide data at precisely $t/T=1$); the left column is for $R=8.6$ cm and the right column is for $R=13.9$ cm; the top row is for $d=1$ mm and the bottom row is for $d=2$ mm. The horizontal dashed lines indicate the unit dimensionless velocity for the tumbler radius and particle size combination (color online). The curve connecting the waveform peaks at different forcing frequencies (red online), indicates the variation in the phase lag of the free surface of the flowing layer. The vertical curve for each forcing frequency (black online) traces the phase lag through the depth.

tumbler rotated at least one full revolution at $Fr=10^{-4}$, the rotational speed was abruptly increased to $Fr=10^{-3}$ and image acquisition began. 20 separate trials were conducted for the four combinations of tumbler radii and particle diameters with similar image processing and ensemble averaging as described earlier.

The response of streamwise velocity for $d=1$ mm particles in the $R=8.6$ cm tumbler is shown in Fig. 8. The solid curve is a fit of the data (after subtracting the initial value and normalizing to the mean) of the general step response function [39] having the form

$$S(t) = 1 - e^{-\rho t} \frac{\sin(\mu t + \Phi)}{\sin \Phi}, \tag{4}$$

where ρ is the damping of the response, μ is the ringing frequency of the response, and Φ is the phase offset. As expected, particles at the free surface have higher acceleration than those deeper in the flowing layer. The form of the response also exhibits dynamic behavior in that the streamwise velocity significantly overshoots the mean velocity generated by the increased rotational speed of the tumbler. It is evident that the damping is significant throughout the flow-
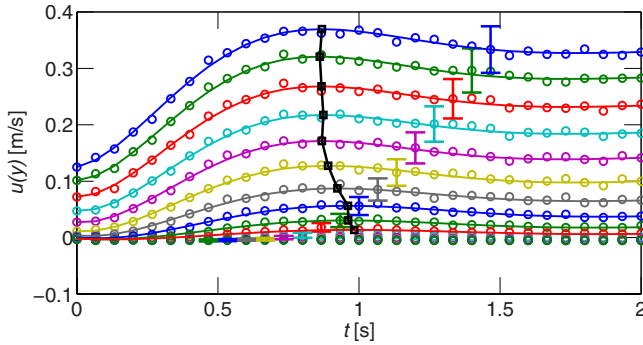
FIG. 8. (Color online) Response of the streamwise velocity for single-particle-diameter-thick layers to a step increase in Fr at time $t=0$ s; $d=1$ mm particles in the $R=8.6$ cm tumbler. Markers represent the raw data with curves corresponding to a fit to the general step response function in Eq. (4). Black square markers and the vertical curve indicate the time of the maximum overshoot of the fitting function. Typical standard deviations are indicated between $0.5 \leq t \leq 1.5$ s.

ing layer with little to no oscillations after the maximum overshoot as the flow quickly settles into a new steady state. However, the time to peak t_P changes through the flowing layer, as indicated by the vertical black curve. The top five layers achieve maximum overshoot within 8 ms of one another, but t_P increases for layers deeper in the flow. The increased time to peak may be a result of those deeper layers previously being part of the fixed bed and having zero streamwise velocity prior to the step change in rotational speed. This suggests that the step response from an initial zero velocity state may be different than the velocity response between two continuous flow conditions, as is the case here.

Figure 9 shows the dimensionless streamwise velocity response at the free surface for all particle-tumbler combinations as a function of the elapsed time from the step increase in rotational speed. The streamwise velocity is nondimensionalized by the steady-state velocity $u_{\text{steady state}}$ at the higher rotational speed. The results indicate that the form and
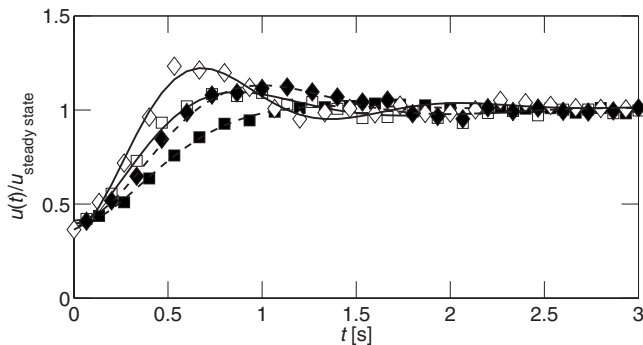

FIG. 9. Streamwise velocity (relative to final velocity) at the free surface as a function of time following a step increase in the rotational speed at $t=0$. ($\square$) $d=1$ mm particles and ($\diamond$) $d=2$ mm particles; open markers represent tumbler radius $R=8.6$ cm and filled markers represent $R=13.9$ cm. For clarity of the fitted step response, markers are only shown for half of the time steps.

TABLE I. Ringing frequency μ (in Hz) and the rise time t_R (in seconds) of the velocity response to a step increase in rotational speed.

Particle size	Tumbler radius	
	$R=8.6$ cm	$R=13.9$ cm
$d=1$ mm	$\mu=0.55$, $t_R=0.41$	$\mu=0.35$, $t_R=0.67$
$d=2$ mm	$\mu=0.73$, $t_R=0.27$	$\mu=0.51$, $t_R=0.42$

magnitude of the overshoot are influenced by the combination of tumbler radius and particle size. In particular, the $R=8.6$ cm tumbler with $d=2$ mm particles generates responses that overshoot the final velocity by over 35% of the change in velocity compared to the $R=13.9$ cm tumbler with $d=1$ mm particles, where the streamwise velocity rises slowly and overshoots the final value by only 3% of the change in velocity. The larger overshoot causes the velocity to oscillate before settling to the new steady streamwise velocity, whereas responses with a small overshoot have virtually no oscillation. For constant particle size, the magnitude of the overshoot decreases with increasing tumbler radius. On the other hand, for constant tumbler radius, the magnitude of overshoot increases with increasing particle size. One possible interpretation is that increasing the number of particle contacts (smaller particles and larger tumbler) increases the "damping" of energy at higher frequencies resulting from the step change in the tumbler rotational speed. This damping reduces the magnitude of the overshoot and also creates an increased time lag relative to the input.

This time lag is also reflected in the dynamic parameters of ringing frequency μ and rise time t_R, which is the time for the velocity response to transition from 10–90% of the total change in velocity. Table I shows the value of these dynamic parameters for the free-surface velocity response. The inverse relationship between these two parameters is evident. The ringing frequency decreases with increasing tumbler radius and increases with increasing particle size. Conversely, the rise time increases with increasing tumbler radius and decreases with increasing particle size. Of course, more combinations of system level parameters are necessary to better characterize the dynamic response to a step input such that a ringing frequency could be directly related to the system resonance. Nonetheless, the streamwise velocity response to step increases in the rotational speed exhibits behavior consistent with the response to the periodic forcing protocol: a damped resonancelike oscillatory response in the form of an overshoot and a time lag to reach new steady-state flow conditions.

IV. CONCLUSIONS

These experiments clearly demonstrate the dynamics of the response of a granular system to transient forcing. The velocity response throughout the flowing layer mimics the form of the forcing by the rotational speed of the tumbler, be it a periodic input or a step input. As the periodic forcing frequency of the tumbler rotational speed increases, the flow

of the granular material responds with increasing phase lag, reflecting the time that is required to transmit external operating conditions to the interior flowing regions of the tumbler. A similar lag occurs in the response to step changes in the rotational speed of the tumbler. Varying the tumbler radius and particle diameter indicates that a greater number of interparticle contacts (large radius, small particle) causes greater phase lag, while fewer contacts (small tumbler radius, large particles) result in a reduced phase lag. This is likely related to the way that networks of particle contacts transmit forces as the number of contacts changes. Though the phase lag has not been included in models of the flow [25,33], the impact is minimal for small values of the forcing frequency and the delay in the flow velocity is usually unimportant in circular tumblers due to the flowing layer length being independent of the angular orientation. The phase lag property plays a role in circular tumblers if the location of the segregated lobes is required relative to a fixed point on the tumbler or in polygon-shaped tumblers, where the change in the flowing layer length can be abrupt.

The amplitude of the dynamic response of the flow for periodic forcing has characteristics of a resonant behavior. It may be possible to exploit this result to determine optimal operating conditions for transporting granular materials or possibly provide means of predicting energy dissipation resulting from interparticle collisions. Step changes in the forcing sometimes result in overshoot behavior, indicating that forces and acceleration of particles may exceed those observed in steady-state conditions. This may be important for granular processing operations that are not continuous to avoid high forces that may damage machinery or the particles themselves.

This paper primarily focuses on relatively simple forcing of a granular flow in a rotating tumbler. It would be profitable to explore higher amplitude or multiple frequency forcing to further understand the dynamic response of a granular flow. In fact, the dynamic response to transient operating conditions may create a new avenue for rheological characterization and understanding of granular flow behavior. Transient flows may provide an additional component for full characterization of size distribution, moisture content, or other properties of raw granular materials.

[1] D. Bonn, S. Rodts, M. Groenink, S. Rafai, N. Shahidzadeh-Bonn, and P. Coussot, Annu. Rev. Fluid Mech. **40**, 209 (2008).

[2] N. Jain, J. M. Ottino, and R. M. Lueptow, Phys. Fluids **14**, 572 (2002).

[3] S. W. Meier, R. M. Lueptow, and J. M. Ottino, Adv. Phys. **56**, 757 (2007).

[4] *Jamming and Rheology*, edited by A. J. Liu and S. R. Nagel (Taylor & Francis, London, 2001).

[5] GDR MiDi, Eur. Phys. J. E **14**, 341 (2004).

[6] P. Chen, J. M. Ottino, and R. M. Lueptow, Phys. Rev. E **78**, 021303 (2008).

[7] G. H. Ristow, *Pattern Formation in Granular Materials* (Springer, New York, 2000), Vol. 164.

[8] K. M. Hill, G. Gioia, and V. V. Tota, Phys. Rev. Lett. **91**, 064302 (2003).

[9] A. A. Boateng and P. V. Barr, J. Fluid Mech. **330**, 233 (1997).

[10] O. Pouliquen and N. Renaut, J. Phys. II **6**, 923 (1996).

[11] P. Jop, Y. Forterre, and O. Pouliquen, Phys. Fluids **19**, 088102 (2007).

[12] S. Courrech du Pont, R. Fischer, P. Gondret, B. Perrin, and M. Rabaud, Phys. Rev. Lett. **94**, 048003 (2005).

[13] W. Losert and G. Kwon, Adv. Complex Syst. **4**, 369 (2001).

[14] B. Utter and R. P. Behringer, Eur. Phys. J. E **14**, 373 (2004).

[15] M. Toiya, J. Stambaugh, and W. Losert, Phys. Rev. Lett. **93**, 088001 (2004).

[16] P. Jalali, J. Ritvanen, and P. Sarkomaa, Exp. Fluids **39**, 554 (2005).

[17] A. Santomaso, P. Lazzaro, and P. Canu, Chem. Eng. Sci. **58**, 2857 (2003).

[18] E. Ben-Naim, J. B. Knight, E. R. Nowak, H. M. Jaeger, and S. R. Nagel, Physica D **123**, 380 (1998).

[19] X. Cheng, R. Smith, H. M. Jaeger, and S. R. Nagel, Phys. Fluids **20**, 123305 (2008).

[20] W. C. Saeman, Chem. Eng. Prog. **47**, 508 (1951).

[21] S. Das Gupta, D. V. Khakhar, and S. K. Bhatia, Powder Technol. **67**, 145 (1991).

[22] S.-Q. Li, J.-H. Yan, R.-D. Li, Y. Chi, and K.-F. Cen, Powder Technol. **126**, 217 (2002).

[23] S.-Q. Li, Y. Chi, R.-D. Li, J.-H. Yan, and K.-F. Cen, Powder Technol. **126**, 228 (2002).

[24] D. V. N. Prasad and D. V. Khakhar, Phys. Rev. E **77**, 041301 (2008).

[25] S. J. Fiedor and J. M. Ottino, J. Fluid Mech. **533**, 223 (2005).

[26] S. W. Meier, D. A. M. Barreiro, J. M. Ottino, and R. M. Lueptow, Nat. Phys. **4**, 244 (2008).

[27] K. M. Hill, G. Gioia, D. Amaravadi, and C. Winter, Complexity **10**, 79 (2005).

[28] K. M. Hill, A. Caprihan, and J. Kakalios, Phys. Rev. E **56**, 4386 (1997).

[29] S. J. Fiedor and J. M. Ottino, Phys. Rev. Lett. **91**, 244301 (2003).

[30] S. J. Fiedor, P. Umbanhowar, and J. M. Ottino, Phys. Rev. E **76**, 041303 (2007).

[31] K. Choo, M. W. Baker, T. C. A. Molteno, and S. W. Morris, Phys. Rev. E **58**, 6115 (1998).

[32] K. M. Hill, D. V. Khakhar, J. F. Gilchrist, J. J. McCarthy, and J. M. Ottino, Proc. Natl. Acad. Sci. U.S.A. **96**, 11701 (1999).

[33] S. W. Meier, S. E. Cisar, R. M. Lueptow, and J. M. Ottino, Phys. Rev. E **74**, 031310 (2006).

[34] N. A. Pohlman, J. M. Ottino, and R. M. Lueptow, Phys. Rev. E

74, 031305 (2006).

[35] E. A. Cowen and S. G. Monismith, Exp. Fluids **22**, 199 (1997).

[36] A. V. Orpe and D. V. Khakhar, Phys. Rev. Lett. **93**, 068001 (2004).

[37] A. V. Orpe and D. V. Khakhar, Phys. Rev. E **64**, 031302

(2001).

[38] H. Henein, J. K. Brimacombe, and A. P. Watkinson, Metall. Trans. B **14**, 191 (1983).

[39] G. F. Franklin, J. D. Powell, and A. Emami-Naeini, *Feedback Control of Dynamic Systems*, 3rd ed. (Addison-Wesley, Reading, MA, 1994).